Dimensional Crossover in Thermal Radiation: From 3D to 2D Heat Transfer between Metallic Membranes

Jose Ordonez-Miranda, Roman Anufriev, Masahiro Nomura, Sebastian Volz

Dimensional Crossover in Thermal Radiation: From 3D to 2D Heat Transfer between Metallic Membranes

Jose Ordonez-Miranda,[1,2,*] Roman Anufriev,[1,3] Masahiro Nomura,[2,1] and Sebastian Volz[1,2]

[1] *LIMMS, CNRS-IIS IRL 2820, The University of Tokyo, Tokyo 153-8505, Japan*
[2] *Institute of Industrial Science, The University of Tokyo, Tokyo 153-8505, Japan*
[3] *CETHIL, Univ. Lyon, INSA Lyon, CNRS, UMR5008, 69621 Villeurbanne, France*

(Dated: September 6, 2024)

Based on fluctuational electrodynamics, we reveal a dimensional crossover in far-field thermal radiation between subwavelength gold membranes. As the membrane thickness decreases from bulk to nanoscale, we observe a transition from three-dimensional (3D) to two-dimensional (2D) heat transfer, characterized by a distinct minimum plateau in thermal conductance for intermediate subwavelength thicknesses. This behavior, absent in polar dielectrics, stems from the coupling and decoupling of long-range surface plasmon-polariton modes. The thermal conductance exhibits a T^3 dependence for thick membranes at high temperature and transitions to a T^2 dependence for ultrathin films at low temperature, reflecting the dimensional shift in photon density of states. Notably, the minimum plateau falls below the black body limit, demonstrating the potential for tailoring far-field thermal radiation in metallic nanostructures through dimensional confinement and plasmonic effects.

Thermal radiation through vacuum gaps has attracted significant interest of physicists for several decades [1]. This research field has particularly gained momentum since the 2000s, due to its potential applications to enhance radiative currents and generate passive cooling. In polar materials, the near-field heat flux can exceed the conventional Planck's predictions by several orders of magnitude and is characterized by a very narrow spectrum of photons [2–6]. This substantial enhancement is attributed to the coupling between the evanescent tails of surface waves traveling along the radiating surfaces. These electromagnetic waves are called Surface Phonon-Polaritons (SPhPs) and Surface Plasmon-Polaritons (SPPs) when they are propagate along the surfaces of polar dielectrics and metals, respectively. Both of these surface energy carriers can travel distances of a few millimeters with infrared frequencies that are relevant for room temperature applications [7].

In 2005, SPhPs were also identified as in-plane heat carriers propagating along polar nanofilms [8]. The SPhP heat transport along the interfaces of a SiO_2 film thinner than 50 nm can surpass the vibrational heat conduction at 500 K. This prediction was experimentally confirmed fourteen years later [9, 10]. In the same period, Thompson et al. [11] demonstrated the existence of an unexpectedly high radiative heat flux between two SiN nanofilms separated by a gap of 20 μm. This enhanced far-field radiation is driven by the SPhP propagation along polar nanofilms with a subwavelength thickness and was demonstrated to also exist in the near-field regime [12]. Decreasing the film thickness thus revealed a transition from a three-dimensional (3D) to a two-dimensional (2D) radiation [13], the former becoming substantially weaker than the latter for nanofilms thinner than 1 μm. More recently in 2023, the in-plane SPP heat transport along a single metallic film was also demonstrated [14, 15], though the physical mechanisms in metals differ from the ones in polar materials [16]. However, the SPP contribution to the thermal radiation between two subwavelength films has not been explored yet, despite its importance for practical applications.

In this Letter, we use fluctuational electrodynamics and Maxwell's equations to demonstrate that the far-field radiation between two gold subwavelength membranes is driven by the in-plane propagation of SPPs. The coupling of these plasmonic energy carriers propagating along the top and bottom surfaces of thin membranes increases their radiative thermal conductance. As the thickness increases through intermediate subwavelength values, this SPP coupling weakens and disappears, causing the thermal conductance to reduce until reaching a plateau. This enhancement and minimum plateau are unique features of the thermal radiation between metallic membranes, as they are not present for dielectric membranes [6, 11, 12].

Let us consider two metallic membranes exchanging heat by thermal radiation due to their temperature difference ΔT, as shown in Fig. 1. The lateral dimensions $(l, a) = (80, 20)\mu$m of the identical membranes were chosen big enough to ensure a sizable heat exchange and small enough to keep the calculations tractable. The separation distance was fixed at $g = 20$ μm to ensure the regime of far-field radiation ($g > \lambda_{th}$) above room temperature. According to fluctuational electrodynamics, the net heat flux between the membranes is given by [17, 18]

$$q = \int_0^\infty \hbar\omega \left[f_\omega(T + \Delta T) - f_\omega(T) \right] \Phi(\omega) d\omega, \qquad (1)$$

where ω is the radiation frequency, $f_\omega(T) = \left[\exp\left(\hbar\omega/k_B T\right) - 1\right]^{-1}$ is the Bose-Einstein distribution

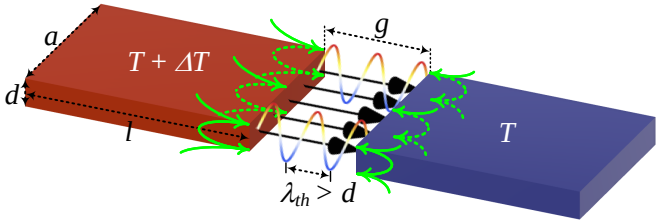

FIG. 1: Scheme of two subwavelength membranes exchanging far-field thermal radiation through photons (wavy lines) and SPPs (green lines). The photons are emitted from the facing surfaces, while the SPPs are radiated after propagating along the top and bottom surfaces. The membranes are identical and their red and blue colors indicate high $(T + \Delta T)$ and low (T) temperature, respectively. The thickness d is smaller than the Wien's wavelength λ_{th}, which is around 10 μm at 300 K. Black arrows represent the direction of the total heat flux.

function, $\hbar$ and k_B are the respective reduced Planck and Boltzmann constants, and Φ is the transmission function of the random currents' energy from the left membrane (emitter) into the right one (receiver). We determine Φ by using the boundary-element method, a mature and sophisticated formulation in which the electromagnetic fields are calculated from the fluctuations of surface currents [18]. This method has been extensively applied to study near-field and far-field thermal radiation and we used it via the free-software solver Scuff-EM. For the sake of simplicity and conciseness, we evaluate q through the thermal conductance $G = q/\Delta T$, which for a temperature difference $\Delta T \ll T$ and the linear approximation of $f_\omega(T + \Delta T) \approx f_\omega(T) + \Delta T \partial f_\omega(T)/\partial T$, becomes independent of ΔT and is determined by

$$G = \int_0^\infty \hbar\omega \frac{\partial f_\omega(T)}{\partial T} \Phi(\omega) d\omega. \qquad (2)$$

The Scuff-EM calculations were done by discretizing both membranes into surface elements, as shown in Fig. S12(a) of the Supplementary Material (SM) [19]. The meshing was chosen sufficiently fine to generate 28048 fluctuational surface currents, ensuring the transmission function convergence for frequencies up to 100 THz. All calculations were done for membranes of gold, which is a good SPP conductor due to its high plasma frequency ($\omega_p/2\pi$ = 2196.3 THz) and relatively low absorption (damping factor = $\Gamma/2\pi$ = 15.9 THz) [20] enabling the long-range propagation of SPPs over a wide frequency range [14]. For temperatures lower than 500 K and thicknesses greater than 25 nm, these values of ω_p and Γ are practically independent of the membrane temperature and thickness[21, 22], and they allow the Drude model used in our calculations to describe well the gold permittivity for frequencies up to 100 THz [23]. Unlike the real part of the permittivity of polar materials, the one of gold is large and negative for all frequencies lower than ω_p (see Fig. S9 of the SM [19]), which favors the existence and propagation of SPPs over a relatively broad range of frequencies. The thermal excitation and propagation of SPPs in gold membranes is thus expected to enhance the radiative heat transfer via their energy emission at the membranes' edges.

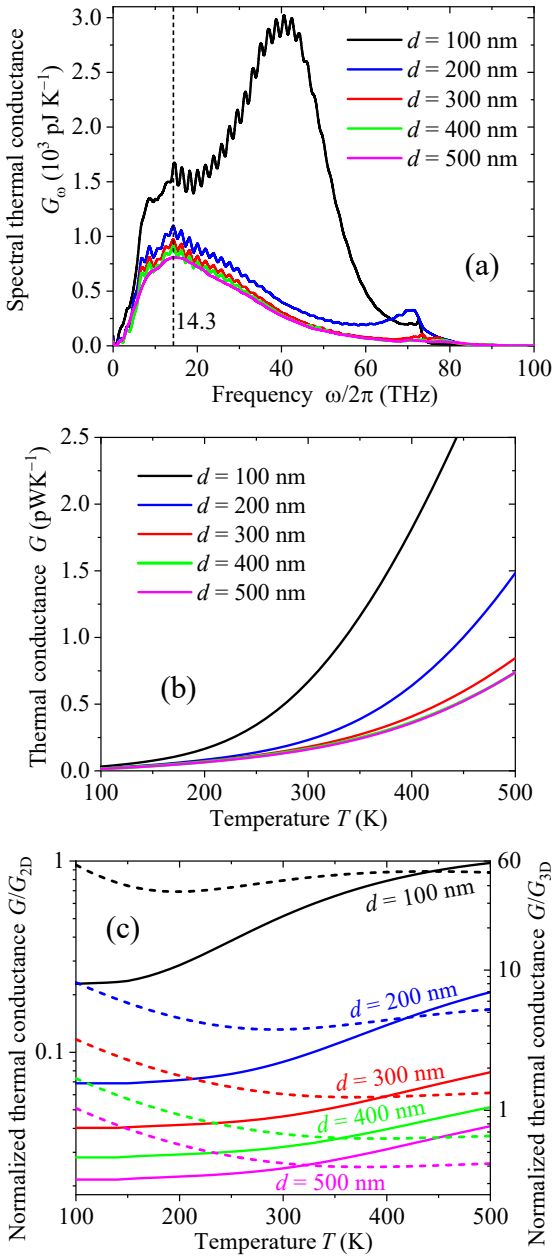

FIG. 2: (a) Spectral thermal conductance between two gold membranes at $T = 300$ K. (b) Temperature evolution of the thermal conductance and (c) its normalized values with respect to the 2D (solid lines) and 3D (dashed lines) thermal conductances predicted by Eqs. (3a) and (3b) for black bodies.

The spectral thermal conductance G_ω is shown in Fig. 2(a) for $T = 300$ K and five representative thicknesses. The tiny ripples of G_ω are caused by the numerical determination of Φ, however they do not significantly impact on our results due to their relatively small amplitude. As the thickness d increases, G_ω decreases and tends to converge with a peak at 14.3 THz, for $d > 500$ nm. Unlike the spectral thermal conductance for SiN membranes [11], the one for gold membranes takes higher values for smaller thicknesses, especially when d reduces from 200 to 100 nm. This counterintuitive enhancement and convergence of G_ω for deep subwavelength thicknesses, leads to a thermal conductance $G = \int G_\omega d\omega$ with the same behavior, as shown in Fig. 2(b), as a function of temperature. Higher G values are obtained for thinner and hotter membranes. For $T < 200$ K, the thermal conductance $G \propto T^2$, which transforms to $G \propto T^3$, for $T > 400$ K, as demonstrated by its normalization with respect to the following 3D and 2D thermal conductances for two black bodies (see Fig. 2(c) and section S1 of the SM [19])

$$G_{3D} = 4adF_{12}\sigma_{3D}T^3, \tag{3a}$$

$$G_{2D} = 3aF_{12}\sigma_{2D}T^2. \tag{3b}$$

where $\sigma_{3D} = 2\pi^5 k_B^4/(15c^2h^3) = 5.67 \cdot 10^{-8}$ Wm^{-2}K^{-4} and $\sigma_{2D} = 8z(3)k_B^3/(ch^2) = 1.92 \cdot 10^{-10}$ Wm^{-1}K^{-3} are the 3D and 2D Stefan-Boltzmann constants, and F_{12} is the geometrical view factor given in supplementary Eq. (S8a) for the membranes shown in Fig. 1 [24]. This characteristic temperature dependence of G_{3D} and G_{2D} arises from a 3D and 2D density of photon states, respectively; and therefore it represents the fingerprint of the dimensionality of the thermal radiation. The proportionality $G \propto T^n$ shown in Fig. 2(c) thus indicates that the radiation is driven by the 2D ($n = 2$) and 3D ($n = 3$) emission of photons for sufficiently low and high temperatures, respectively. The regime of 2D radiation appears from the linear dependence of the transmission function ($\Phi \propto \omega$ in the supplementary Fig. S12(b)) at low frequencies relevant for low temperatures. According to Eq. (2), this linear behavior leads to the quadratic dependence of $G_\omega \propto \omega^2$, resulting in $G \propto T^2$. For relatively high frequencies, on the other hand, $\Phi \propto \omega^2$ and therefore $G_\omega \propto \omega^3$ ($G \propto T^3$), which drives the usual 3D radiation. The 2D (in-plane) far-field radiation between gold subwavelength membranes also appears in the near-field radiation between SiN membranes, as we show in the supplementary Fig. S11(b) that we obtained by using experimental data recently reported by Luo *et al.* [12]. These authors explained their measurements through the in-plane propagation of SPhPs along the SiN membranes, which suggests that our low-temperature results shown in Figs. 2(a) and 2(b) could be driven by SPPs propagating along the top and bottom surfaces of the gold membranes. This suggestion is reinforced by the fact that the quantum of thermal conductance per unit width of polaritons propagating along a single nanofilm also increases with T^2 and is equal to $G_{2D}/(2aF_{12})$ [25]. The factor two is explained by the contribution of two modes to G_{2D}, as detailed in section S1 of the SM [19].

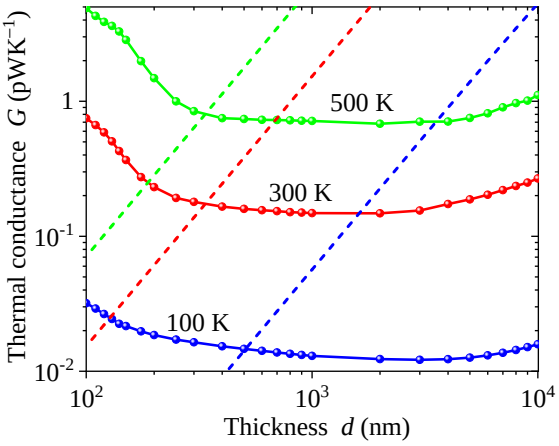

FIG. 3: Thermal conductance between two gold membranes as a function of their thickness. The dashed lines stand for the 3D black body radiation predicted by Eq. (3a). Calculations were done for three representative temperatures.

Figure 3 shows the computed thermal conductance G as a function of the membranes' thickness d. Note that G becomes independent of d and takes values lower than the 3D black body limit, within an interval of intermediate thicknesses smaller than the Wien's wavelength $\lambda_{th} = 2897.77/T$ µm. The minimum plateau of G thus appears for subwavelength thicknesses that increase when the temperature decreases. This plateau indicates that the obtained heat transfer rate is not determined by the cross-section area of the radiating membranes or their view factor determining the 3D thermal radiation. Further, the behavior of G is consistent with that of the emissivity of a gold membrane, which takes higher values for membranes thinner than 100 nm and becomes independent of the thickness for thicker membranes, as shown in supplementary Fig. S10 [19, 26].

Considering that the gold membranes support not only the emission of photons, but also the propagation of SPPs along their top and bottom surfaces, we analyze the impact of these energy carriers on the obtained thermal conductance. According to the supplementary section S2 [19], the solution of the Maxwell equations for the transverse magnetic (TM) polarization supporting the long-range propagation of SPPs establishes that they propagate along a single membrane with the following in-plane

(β) and cross-plane (p_1, p_2) wave vectors[27]

$$\beta = \sqrt{\varepsilon_1} k_0 \sqrt{1 + \frac{\varepsilon_1}{\varepsilon_2}\gamma^{\pm 2}}, \tag{4a}$$

$$p_1 = \pm \frac{\varepsilon_1 k_0}{\sqrt{\varepsilon_2}} \gamma^{\pm 1}, \quad p_2 = k_0 \sqrt{-\varepsilon_2}, \tag{4b}$$

where ε_2 and $\varepsilon_1 = 1$ are the respective relative permittivities of a gold membrane and its surrounding vacuum, $k_0 = \omega/c$ and c are the corresponding wave vector and speed of light in vacuum, $\gamma = \tan\left(\sqrt{\varepsilon_2} k_0 d/2\right)$ and the plus (+) and minus (−) signs in ± correspond to the even (EM) and odd (OM) TM modes, respectively. Both TM modes propagate inside the membrane with the same wave vector p_2 independent of thickness due to the relatively high permittivity of gold ($|\varepsilon_2| \sim 10^4$) compared to that of vacuum [19]. Outside the membrane, the wave vector p_1 does depend on the membrane thickness via γ, as is the case of the in-plane wave vector β inside and outside the membrane. However, taking into account the equality $\tan(x+iy) = [\tan(x) + i\tanh(y)]\,/\,[1 - i\tan(x)\tanh(y)] = i$ for $\tanh(y) = 1$, which is well satisfied for $y > 2$; the parameter $\gamma = i$ for $k_0 d \mathrm{Im}(\sqrt{\epsilon_2}) > 4$. In this case, Eqs. (4a) and (4b) establish that the in-plane ($\beta = \sqrt{\varepsilon_1} k_0 \sqrt{1 - \varepsilon_1/\varepsilon_2}$) and cross-plane ($p_1 = i\varepsilon_1 k_0/\sqrt{\varepsilon_2}$) wave vectors of the even and odd modes are equal and independent of the membrane thickness. This thickness and mode independence of the three wave vectors shows up for $d > 4\left[k_0 \mathrm{Im}(\sqrt{\varepsilon_2})\right]^{-1} = 4\left[k_0 \mathrm{Re}(\sqrt{-\varepsilon_2})\right]^{-1} = 8\delta_2$ eight times greater than the SPP penetration (skin) depth $\delta_2 = [2\mathrm{Re}\,(p_2)]^{-1}$ inside the membrane [19]. According to Fig. S5(b) of the SM, $\delta_2 \lesssim 25$ nm, for all frequencies with a relevant contribution to G_ω (see Fig. 2(a)), and therefore the SPP modes propagating along the top and bottom surfaces are expected to decouple in gold membranes thicker than 200 nm. For these thick relatively membranes, G also becomes independent of thickness (see Fig. 3), which links the minimum plateau of the thermal radiation with the SPP modes' decoupling.

The in-plane ($\Lambda = [2\mathrm{Im}(\beta)]^{-1}$) and cross-plane ($\Lambda_1 = [2\mathrm{Re}(p_1)]^{-1}$) propagation length of the even and odd modes are respectively shown in Figs. 4(a) and 4(b) as functions of thickness. For the three frequencies relevance for G_ω, the even mode propagates longer in-plane and cross-plane distances than the odd mode, such that they converge to a common value independent of thickness, for $d > 200$ nm. The values of Λ for both modes are three orders of magnitude longer than the respective Λ_1, which highlights the ability of SPPs to transport and confine their energy over relatively long distances along the membranes' surfaces. As the membrane thickness reduces, the relative increase of Λ(EM) and Λ_1(EM) is greater than the corresponding decrease of Λ(OM) and Λ_1(OM), and therefore the even mode leads the in-plane and cross-plane propagation of the SPP energy. This fact

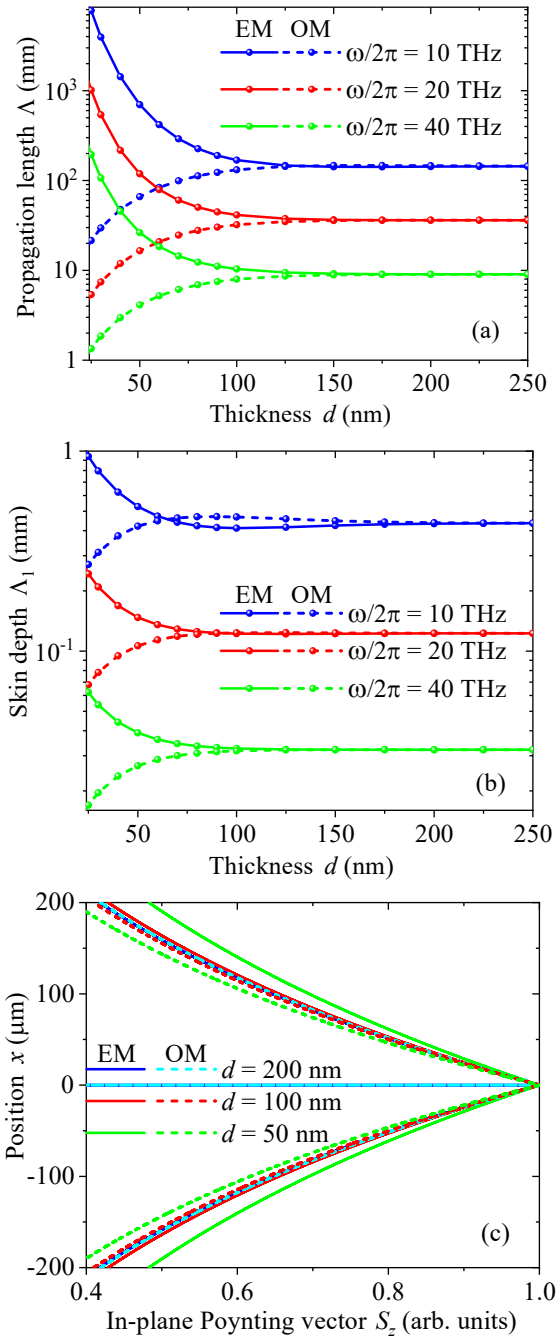

FIG. 4: (a) In-plane and (b) cross-plane (skin depth) propagation lengths of the even and odd modes of SPPs propagating along a single gold membrane, as functions of its thickness. (c) Spatial distribution of the corresponding energy density (Poynting vector) propagating with the peak frequency $\omega/2\pi = 14.3$ THz of the spectral thermal conductance shown in Fig. 2(a). Calculations were done for three representative frequencies and thicknesses for the thermal conductance shown in Figs. 2 and 3.

is confirmed by the spatial distribution of the Poynting

vector shown in Fig. 4(c), which shows that the energy density of the even mode is distributed in a larger cross-section area than that of the odd mode, for $d < 200$ nm. For thicker membranes, the energy density of both modes converges to the same line and keeps confined along the membrane surfaces mainly. This thickness convergence and surface confinement confirm that the propagation of SPPs along a single gold membrane determines the minimum plateau of the radiative thermal conductance across two membranes of thickness $d > 200$ nm. For thinner membranes, the increase of G is explained by the dominant role of the even mode, whose energy propagates longer in-plane distances in larger cross-section areas than the odd mode. This fact is further ratified by the spatial distribution of the Poynting vector magnitude shown in Figs. 5(a) and 5(b) around the radiating surfaces of membranes with thicknesses of 100 and 500 nm, respectively. Note that the left membrane emits its electromagnetic energy flux from a cross-section area larger than its geometrical one and larger for thinner membranes. Even though most of the energy propagates inside the emitter, this enlargement at its boundary is generated by the concentration of energy propagating outside the emitter. The receiver (right membrane) absorbs the energy in a relatively small cross-section area that coincides with its geometrical one, for thick enough membranes ($d = 500$ nm). Further, the effective cross-sections of the emitter and receiver become independent of thickness, for thicknesses greater than 200 nm, confirming the radiative thermal conductance plateau between the gold membranes.

In summary, we have demonstrated that the far-field thermal radiation between two subwavelength gold membranes reaches a minimum plateau that falls below the black body limit. This plateau predicted by fluctuational electrodynamics results from the decoupling of two long-range and ultrafast modes of SPPs propagating along the radiating membranes. The temperature evolution of the computed thermal conductance is well described by the combined emission of photons with a three-dimensional and two-dimensional density of states. Unlike the far-field radiation between subwavelength polar dielectrics, the one between gold membranes increases for membranes thinner than 200 nm. Our findings thus uncover the potential of SPPs to enhance and control the far-field thermal radiation between metallic nanofilms.

This work was supported by the CREST JST (Grant number JPMJCR19I1) and KAKENHI JSPS (Grant number 21H04635 and JP20J13729) projects, as well as by the JSPS Core-to-Core Program (Grant number: JPJSCCA20190006).

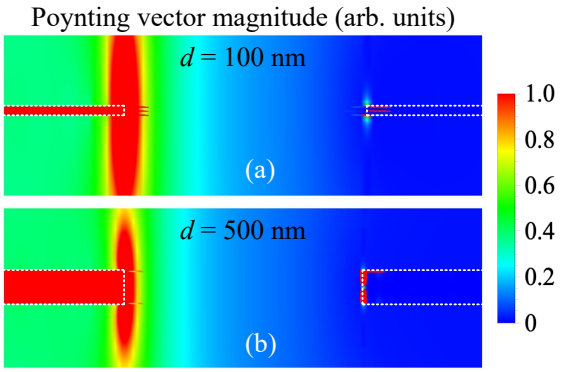

FIG. 5: Density map of the Poynting vector magnitude between two gold membranes with a thickness of (a) 100 nm and (b) 500 nm. Calculations were done at the middle (half width $y = a/2$) of the membranes and for the peak frequency $\omega/2\pi = 14.3$ THz of the spectral thermal conductance shown in Fig. 2(a). The thinner left membrane emits its energy with a larger cross-section area than the thicker left membrane. The three horizontal lines near the edge of the left membrane in (a) and the sharp red lines near the edge of the right membranes are minor numerical artifacts, as they appear in scales that go beyond the resolution of our numerical calculations.

* jose.ordonez@cnrs.fr

[1] D. Polder and M. Van Hove, Theory of radiative heat transfer between closely spaced bodies, Phys. Rev. B **4**, 3303 (1971).
[2] J. J. Loomis and H. J. Maris, Theory of heat transfer by evanescent electromagnetic waves, Phys. Rev. B **50**, 18517 (1994).
[3] K. Joulain, J.-P. Mulet, F. Marquier, R. Carminati, and J.-J. Greffet, Surface electromagnetic waves thermally excited: Radiative heat transfer, coherence properties and casimir forces revisited in the near field, Surf. Sci. Rep. **57**, 59 (2005).
[4] E. Rousseau, A. Siria, G. Jourdan, S. Volz, F. Comin, J. Chevrier, and J.-J. Greffet, Radiative heat transfer at the nanoscale, Nature Photonics **3**, 514 (2009).
[5] S. Shen, A. Narayanaswamy, and G. Chen, Surface phonon polaritons mediated energy transfer between nanoscale gaps, Nano Lett. **9**, 2909 (2009).
[6] B. Song, D. Thompson, A. Fiorino, Y. Ganjeh, P. Reddy, and E. Meyhofer, Radiative heat conductances between dielectric and metallic parallel plates with nanoscale gaps, Nature Nanotechnology **11**, 509 (2016).
[7] J. Ordonez-Miranda, L. Tranchant, B. Kim, Y. Chalopin, T. Antoni, and S. Volz, Quantized thermal conductance of nanowires at room temperature due to zenneck surface-phonon polaritons, Phys. Rev. Lett. **112**, 055901 (2014).
[8] D.-Z. A. Chen, A. Narayanaswamy, and G. Chen, Surface phonon-polariton mediated thermal conductivity en-

hancement of amorphous thin films, Phys. Rev. B **72**, 155435 (2005).

[9] L. Tranchant, S. Hamamura, J. Ordonez-Miranda, T. Yabuki, A. Vega-Flick, F. Cervantes-Alvarez, J. J. Alvarado-Gil, S. Volz, and K. Miyazaki, Two-dimensional phonon polariton heat transport, Nano Lett. **19**, 6924–6930 (2019).

[10] Y. Wu, J. Ordonez-Miranda, S. Gluchko, R. Anufriev, D. D. S. Meneses, L. D. Campo, S. Volz, and M. Nomura, Enhanced thermal conduction by surface phonon-polaritons, Sci. Adv. **6**, eabb4461 (2020).

[11] D. Thompson, L. Zhu, R. Mittapally, S. Sadat, Z. Xing, P. McArdle, M. M. Qazilbash, P. Reddy, and E. Meyhofer, Hundred-fold enhancement in far-field radiative heat transfer over the blackbody limit, Nature **561**, 216 (2018).

[12] X. Luo, H. Salihoglu, Z. Wang, Z. Li, H. Kim, X. Liu, J. Li, B. Yu, S. Du, and S. Shen, Observation of near-field thermal radiation between coplanar nanodevices with subwavelength dimensions, Nano Letters **24**, 1502 (2024).

[13] S. Tachikawa, J. Ordonez-Miranda, L. Jalabert, Y. Wu, R. Anufriev, Y. Guo, B. Kim, H. Fujita, S. Volz, and M. Nomura, Enhanced far-field thermal radiation through a polaritonic waveguide, Phys. Rev. Lett. **132**, 186904 (2024).

[14] J. Ordonez-Miranda, Y. A. Kosevich, B. J. Lee, M. Nomura, and S. Volz, Plasmon thermal conductance and thermal conductivity of metallic nanofilms, Phys. Rev. Appl. **19**, 044046 (2023).

[15] D.-M. Kim, S. Choi, J. Cho, M. Lim, and B. J. Lee, Boosting thermal conductivity by surface plasmon polaritons propagating along a thin ti film, Phys. Rev. Lett. **130**, 176302 (2023).

[16] P.-O. Chapuis, S. Volz, C. Henkel, K. Joulain, and J.-J. Greffet, Effects of spatial dispersion in near-field radiative heat transfer between two parallel metallic surfaces, Phys. Rev. B **77**, 035431 (2008).

[17] S. Basu, Z. M. Zhang, and C. J. Fu, Review of near-field thermal radiation and its application to energy conversion, Int. J. Energy Res. **33**, 1203 (2009).

[18] A. W. Rodriguez, M. T. H. Reid, and S. G. Johnson, Fluctuating-surface-current formulation of radiative heat transfer: Theory and applications, Phys. Rev. B **88**, 054305 (2013).

[19] S. the Supplemental Material at xyz, for the detailed derivation of the dispersion relation and poynting vector of sphps, as well as the intracavity thermal radiation predicted by planck's law, .

[20] A. Alabastri, S. Tuccio, A. Giugni, A. Toma, C. Liberale, G. Das, F. D. Angelis, E. D. Fabrizio, and R. P. Zaccaria, Molding of plasmonic resonances in metallic nanostructures: Dependence of the non-linear electric permittivity on system size and temperature, Materials **6**, 4879 (2013).

[21] M.-L. Thèye, Investigation of the optical properties of au by means of thin semitransparent films, Phys. Rev. B **2**, 3060 (1970).

[22] P. de Vera and R. Garcia-Molina, Electron inelastic mean free paths in condensed matter down to a few electron-volts, J. Phys. Chem. C **123**, 2075 (2019).

[23] A. D. Rakić, A. B. Djurišić, J. M. Elazar, and M. L. Majewski, Optical properties of metallic films for vertical-cavity optoelectronic devices, Appl. Opt. **37**, 5271 (1998).

[24] M. F. Modest, *Radiative Heat Transfer* (Elsevier Science, California, 2003).

[25] Y. Guo, S. Tachikawa, S. Volz, M. Nomura, and J. Ordonez-Miranda, Quantum of thermal conductance of nanofilms due to surface-phonon polaritons, Phys. Rev. B **104**, L201407 (2021).

[26] O. S. Heavens, *Optical Properties of Thin Solid Films* (Dover publications, London, 2011).

[27] C. Yeh and F. I. Shimabukuro, *The Essence of Dielectric Waveguides* (Springer, New York, 2008).